Initial Deposition of Interacting Particles by Filtration of Dilute Suspensions

M. A. "Curt" Koenders
Dept. of Physics, Kingston University, Penrhyn Road, Kingston on Thames, Surrey KT1 2EE, U.K.

Richard J. Wakeman
Dept. of Chemical Engineering, Loughborough University, Ashby Road, Loughborough, Leics. LE11 3TU, U.K.

Data from a range of filtration experiments on dilute suspensions are used to determine the parameters that describe the physics of suspension flow during compaction. The range of solids volume fractions used is $0.00001 < \phi < 0.1$; ζ-potentials vary between 0 and 50 mV. Relevant physical data are extracted from an analysis of the initial stages of experiments at various ϕ and ζ. Theoretical considerations on suspension flow are presented to argue that the physical character of the flow at relatively dense, strongly interacting conditions is significantly different from that of dilute systems. The latter are dominated by fluctuations in the particle velocity near the septum to give gas-type diffusive behavior, while in the former the particles are more or less localized. This observation has implications for the diffusion coefficient, which is predicted to be quadratic in the filtration pressure for very dilute suspensions and which is roughly independent of pressure for mixtures containing strongly interacting particles. Experiments are described and analyzed, and these reinforce the main theoretical insights.

Introduction

Developments in filtration theory have aimed at providing detailed descriptions of fluid motion through a filter cake due to a hydraulic pressure gradient. This gradient causes an interfacial momentum transfer in the form of viscous drag at the particle–fluid interfaces. If the shape or strength of the solids is such that the packing arrangement of particles in the cake can sustain this force without further movement occurring, then the cake is regarded as incompressible. The modeling approaches involved have been well described in several texts, for example, by Tiller (1975), Shirato et al. (1986a,b), Leu (1986), Smiles (1986), and Wakeman (1986). The compressible nature of many filter cakes is recognized in most of these works, but none takes a rigorous approach to the incorporation of appropriate terms into initial force balances in order to describe either particle–particle or particle–fluid interactions other than drag.

This article is concerned with the physical interpretation of the results measured during filtration experiments in which slurries are dewatered by forcing the liquid component through a permeable septum. The diffusion processes that take place near the septum are used to gain insight into suspension flow properties. In particular, the role of the interparticle force arising from interacting ions and electron clouds around the particles affects the overall flow properties. The pH of the suspension is varied in order to influence the character of the interactive force. Experimental results are reported, and a theoretical investigation is conducted to analyze the observed flow phenomena. From a comparison of the laboratory data with theoretical predictions, the phenomenological microscopic parameters of the theory can be determined.

It will be shown that the mechanical flow parameters can be determined from an analytical, quasi-linear theory that describes the initial stage of filtration. Subsequent stages may be obtained by solving the relevant nonlinear equations numerically. During filtration a wide range of solids concentrations is encountered, beginning with a low solidosity slurry and ending with a densely packed cake. In order to derive

the flow parameters from the initial stage of an experiment, a set of tests is needed to encompass a wide range of initial suspension solidosities at the beginning of each test.

The analysis of the mechanical processes that take place is qualitatively summarized as follows:

1. At the initial stage of the experiment a steep solidosity gradient is generated close to the septum surface, while the septum is clogged by particles settling on it. A force that tends to oppose the gradient works on the particles; this is associated with either an asymmetric charge distribution created around each particle, or with a diffusive effect that arises from the natural fluctuations in the motion of the particles. A large proportion of these fluctuations is generated by the heterogeneous microflow near the septum. Drag forces are investigated; these are due either to the velocity difference between the particles and the fluid that arises as the particle velocity decreases as the particle approaches the deposition surface, or to viscous suspension compression. The force balance of the solid phase, coupled with the two-phase flow equations of continuity, gives a complete set of equations that enable the flow problem to be analyzed. A phenomenological relation is needed to estimate the changes that affect the septum permeability; a relation is used that employs the packing density at the septum surface as the only dynamic parameter (in addition to the static clean water permeability).

2. In the subsequent stages of the compression process, a skeletal stress is created at higher packing densities that flattens the solidosity gradient, thereby forming a cake at the septum.

3. The end phase consists of consolidation of the cake by direct compression.

The latter two phases are not investigated in this article. This article is concerned with the description and analysis of the initial deposition processes and the development of the solidosity gradient immediately after pressure is applied.

The idea that the initial stages of the dewatering process can be used for parameter detection was first suggested by Koenders and Wakeman (1996). The technique requires accurately logged volumetric flow data over a short time scale (during the initial few 100 s, depending on the conditions of the experiment). It has been shown—and will be demonstrated again below in a different manner—that the flow volume for short times behaves as $\mathrm{Vol}(t) = \bar{x}t + \bar{y}t^{3/2}$, where $\bar{x}$ and $\bar{y}$ are system parameters containing information about the applied pressure, the septum resistance, and the influence of membrane fouling, as well as the solidosity-dependent fluid drag and diffusion parameters. Determination of $\bar{x}$ and $\bar{y}$ is accomplished by means of a least-squares procedure, fitting raw experimental time-dependent volumetric flow data to the expected curve. In this way, not only are $\bar{x}$ and $\bar{y}$ obtained, but so are estimated standard deviations in these parameters.

This article is structured as follows. The theory describing particle-interaction-dependent one-dimensional suspension flow is outlined first to determine the relevant constitutive relations. Then the boundary-value problem appropriate to the test setup is discussed for various forms of the interactive particle-pair potential. The experiments are described in some detail, and the constitutive parameters are obtained from these using the least-squares procedure. The experimental data are compared to theoretical predictions, and theoretical concepts are then verified by studying the results of a series of experiments at different initial solidosities and at a range of pressures. This variation in initial conditions yields the information that is required to test the theoretical assumptions.

The results of the analysis are twofold. First, the methodology used for parameter detection is treated and discussed. While the errors in the data obtained are generally quite large, the method gives a reasonable estimate of the relevant parameters that describe the initial cake formation. Second, theoretical considerations of suspension flow are presented to argue that the physical character of the flow at relatively dense, strongly interacting conditions is significantly different from that of dilute systems. The latter are dominated by fluctuations in the particle velocity near the septum, resulting in gas-type diffusive behavior, while in the former the particles are more or less localized. This observation has implications for the diffusion coefficient, which is predicted to behave quadratically in the filtration pressure for very dilute media and which is roughly independent of pressure for mixtures containing strongly interacting particles. These findings are confirmed by the analysis of the experimental data.

Theoretical Investigation

The flow phenomena are described in terms of continuum variables. These are U for the fluid velocity, v for the particle velocity, p for the fluid pressure, and ϕ for the solids volume fraction. All of these are homogenized variables and functions of position x measured from the septum and time t. The experimental piston press is one-dimensional, but for minor effects alongside the vertical walls. The validity of the continuum approach is debatable, because individual particle velocities may vary widely at nearby positions and time points. These fluctuations require continuum variables to be defined over substantial regions of space and over long times; for the fluid itself, the question of the adequacy of the continuum description has been addressed by Murdoch (1983), who demonstrated that material point identification is excellent for molecular length scales. But for the particulate phase the definition of continuum variables should involve many particles in more or less homogeneous circumstances. There is probably no problem when the continuum variables are used to express conservation principles, such as is the case with the equations of continuity. If constitutive properties are evaluated, however, certain nonlocal effects may play a role. In particular, one nonlocal state variable—the granular temperature, which describes the fluctuation intensity evolution of the particle packing, interparticle interactions, and velocity differences between the liquid and solid phases—is needed to obtain the relevant constitutive diffusion relationship. The nonlocal character of the granular temperature implies that the validity range of the model is limited to large length scales, spanning many particle diameters. If any phenomena occur that take place on a short range, an averaging process must be used to ensure that any balance equations operate on the same length scale.

The constitutive behavior of a particle–fluid mixture is required in approximate form in homogenized variables to solve boundary-value problems. The equations of continuity hold in one dimension:

$$\frac{\partial \phi}{\partial t} + \frac{\partial}{\partial x}(\phi v) = 0 \tag{1}$$

$$-\frac{\partial \phi}{\partial t} + \frac{\partial}{\partial x}[(1-\phi)U] = 0. \tag{2}$$

These two equations are for the four field variables U, v, p, and ϕ; the third equation is the constitutive equation for the particulate phase; and the fourth is the constitutive equation for the fluid component of the mixture.

Particle force balance

For the particles a quasi-static force balance, consisting of a particle–fluid interaction and a particle–particle interaction, is proposed. The particle–fluid interaction is of the form:

$$F_{\text{drag}} = V_p \beta (U - v), \tag{3}$$

where β is the ϕ-dependent drag coefficient that is proportional to the viscosity of the fluid μ. The particle volume is denoted by V_p; and the particles have radius a. The functional form of $\beta(\phi)$ is obtained from a fluid-flow model for a medium that consists of solid spheres and fluid in an average isotropic packing. Koenders and Williams (1993) derive a form for $\beta(\phi)$ using no-slip least-squares boundary conditions on neighboring spheres in a fluid-cell model. Happel and Brenner (1973) derive an expression based on the assumption that the outside of the unit cell is frictionless. Both derivations contain approximations, but there is good agreement between the two methods, so an order of magnitude is established for the drag force as a function of the solidosity. The two results are shown in Figure 1.

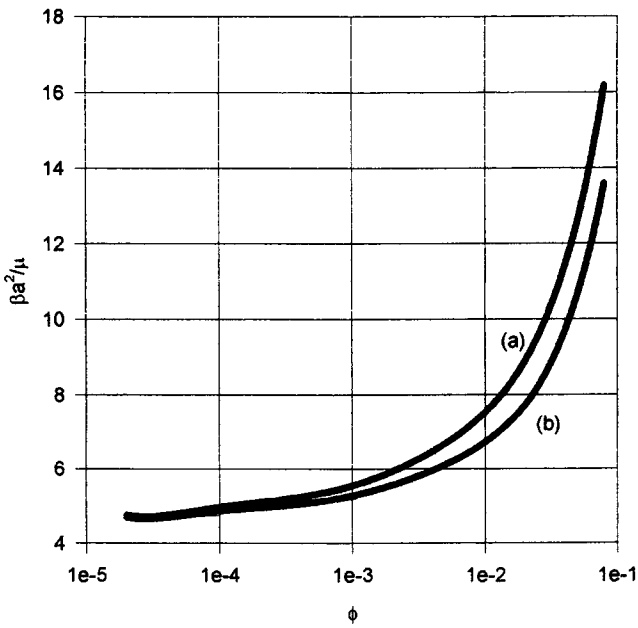

Figure 1. Dimensionless drag coefficient $\beta a^2/\mu$ as a function of the solidosity.

Estimates for isotropic microstructures: (a) according to Koenders and Williams (1992); (b) according to Happel and Brenner (1973).

Another component in the particle–fluid interaction is the compressibility of the suspension that gives rise to the term:

$$F_{\text{comp}} = NV_p \frac{\partial^2 v}{\partial x^2}. \tag{4}$$

This term was also investigated by Koenders and Williams (1993) (for average isotropic packing), and an estimate for N is obtained. Typically N is of the order of magnitude of $n(\phi)\bar{R}^2\beta$, where $n(\phi)$ is a weak function of the solidosity and $\bar{R}$ is the unit cell radius $a\phi^{-1/3}$; $N\bar{R}^{-2}$ is more or less constant as a function of ϕ and is small compared to $\beta(\phi)$. The term given by Eq. 4 is not included in the subsequent analysis (see the Appendix), because for the present filtration problem it only makes a very small contribution to the end result, but requires a disproportionate mathematical effort.

The third force is due to particle–particle interaction (sometimes called *networking*). Buscall and White (1987) utilized the concept of the network possessing a compressive yield stress $P_y(\phi)$, which is assumed to be an implicit function of the strength of the interparticle bridging force and an explicit function of the local volume fraction ϕ of the solids. This implies that $P_y(\phi)$ increases with ϕ due to the larger number of interconnections between particles, and hence the greater strength of the networked structure, and that it becomes vanishingly small below the volume fraction ϕ_g at which the suspension is completely networked (at the gel point). Tentative power-law expressions of the form

$$P_y(\phi) = k_1\left[\left(\frac{\phi}{\phi_g}\right)^{n_1} - 1\right] \quad \text{or}$$

$$P_y(\phi) = k_2\left[\left(\frac{\phi}{\phi_g}\right) - 1\right]^{n_2} \quad (\phi > \phi_g) \tag{5}$$

have been used to fit experimental $P_y(\phi)$ data. Auzerais et al. (1988) used a similar form. In a series of papers Landman et al. (1988, 1991, 1995), Howells et al. (1990), Landman and White (1992), and Landman and Russel (1993) have developed this approach for sedimenting and filtering systems further.

When $P_y(\phi)$ is used, the associated force on a particle is

$$F_{\text{int}} \propto \frac{\partial}{\partial x} P_y(\phi). \tag{6}$$

No networked yield stress is introduced for solidosities less than ϕ_g. These authors employ no compressive force, and while $\phi < \phi_g$, they let the solidosity accumulate linearly with position and time until $\phi = \phi_g$, when the system is determined and the consolidation phase begins. This approach is unsatisfactory for very dilute systems, and the physical processes that control this range need to be investigated further, which we do below.

A more detailed analysis of the particle–particle interaction and the important question of how it is expressed in continuum variables are now explored. The interparticle force for small particles in the 100 nm to 10 μm size range is dominated by the value of the zeta potential. There is a long-range

force for high absolute values at the zeta potential, depending on the particle surface separation h, which has the form $e^{-\kappa h}$. Here κ is the inverse thickness of the double layer, and depending on the electronic conditions, $1/\kappa$ is of the order 0–0.5 μm. The particles used in the experiments described below have a radius of 0.1 to 1 μm and an average separation on the order of 1 μm at $\phi = 0.01$. The effects of the interaction in the parameter range outlined here are therefore important, even at these low concentrations. For small or negligible $1/\kappa$, the functional variation of the force with interparticle separation is quite steep (hard-sphere interaction); for larger values of $1/\kappa$, the behavior is called the soft-sphere interaction. The interactive force can be expanded in a power series in the interparticle surface-separation distance h, involving derivatives of the interactive potential $V(h)$. For increasingly hard interactions, higher order derivatives become relevant (Ottewill, 1980).

We use superscript Greek letters to distinguish the particles. The interactive force is derived from a potential energy function $V(h^{\mu\nu})$; generally speaking, it is a repulsive force, directed along the center lines of the particles. The average particle radius is a. The location of particle μ is $\boldsymbol{x}^{\mu}$; $h^{\mu\nu} = |\boldsymbol{x}^{\mu} - \boldsymbol{x}^{\nu}| - 2a$; and the force $\boldsymbol{F}^{\mu\nu}$ is

$$\boldsymbol{F}_i^{\mu\nu} = -\frac{\partial V(h^{\mu\nu})}{\partial x_i^{\mu}}. \tag{7}$$

The net interactive force on particle μ is

$$\boldsymbol{F}_i^{\mu} = \sum_{\nu \neq \mu} \boldsymbol{F}_i^{\mu\nu} = -\frac{\partial}{\partial x_i^{\mu}} \sum_{\nu \neq \mu} V(h^{\mu\nu}). \tag{8}$$

The situation here is not unlike the one encountered in the statistical mechanics of fluids, with the solid particles playing the role of molecules. The analogy is particularly useful when the hard-sphere interaction applies and a gas-diffusion-type constitutive behavior prevails (see Case 3 below).

For soft-sphere interactions the behavior is more like that of a solid, and the appropriate micromechanical formalism is applied. The interactive net force per unit particle volume $\boldsymbol{F}^{\mu}/V_p$ is derived from a suitably chosen stress $\boldsymbol{\sigma}$ as follows:

$$\frac{\boldsymbol{F}_i^{\mu}}{V_p} = \frac{1}{\phi} \frac{\partial \boldsymbol{\sigma}_{ij}}{\partial x_j}, \tag{9}$$

where the continuum stress is defined as

$$\boldsymbol{\sigma}_{ij} = \frac{1}{\text{volume}} \sum_{\mu} \sum_{\nu \neq \mu} \boldsymbol{F}_i^{\mu\nu} (x_j^{\mu} - x_j^{\nu}). \tag{10}$$

The summation sign over μ is over the particles in the assembly in the volume.

Various cases can be developed and related to the filtration conditions. These cases are distinguished by the aid of the parameter $\kappa^2 \overline{(h - \bar{h})^2}$, measuring the order of magnitude of the fluctuations in the distance between the particles against the range of the interactive force.

Case 1: $\kappa^2 \overline{(h - \bar{h})^2} < 1$. This case concerns a structure where the particles are more or less at rest in a dense packing. The experiments reported below deal with dilute suspensions, and only the initial stage is considered; therefore, this case is developed to elucidate the methodology, and is not verified experimentally.

$V(h)$ is a fast declining function of h and is therefore only able to consider the nearest neighbors. These neighbors will on average be located at a distance $r_0(\vartheta, \varphi, t)$. The summation (Eq. 10) is replaced by an integral over the unit sphere with weighting function $p(\Omega)$, which indicates how many interacting particles are present in a solid angle $d\Omega = \sin\vartheta d\vartheta d\varphi$:

$$\boldsymbol{\sigma}_{ij} = \frac{1}{V_1} \int_{\substack{\text{unit} \\ \text{sphere}}} d\Omega p(\Omega) \boldsymbol{F}_i[r_0(\Omega)] r_0(\Omega) n_j(\Omega), \tag{11}$$

where V_1 represents the volume of the continuum containing a single particle.

Expanding the potential $V(h)$ in a Taylor series yields

$$\boldsymbol{\sigma}_{ij} = \frac{1}{V_1} \int_{\substack{\text{unit} \\ \text{sphere}}} d\Omega p(\Omega) \left\{ \frac{\partial V}{\partial h}\bigg|_{\bar{h}} + \frac{1}{2} \frac{\partial^2 V}{\partial h^2}\bigg|_{\bar{h}} (h - \bar{h}) \right\} \times r_0(\Omega) n_i(\Omega) n_j(\Omega), \tag{12}$$

where $h = r_0(\vartheta, \varphi, t) - 2a$; $\bar{h}$ is the average over time and direction of $r_0(\vartheta, \varphi, t) - 2a$ and is related directly to ϕ (for dense isotropic media—$\phi > 0.2$—the relation between ϕ and $\bar{h}$ is presented by Torquato et al., 1990); and $\boldsymbol{n}$ is a unit-normal vector. Because of the flow direction there is a possible induced anisotropy that has a major principal axis in the x-direction. Thus $r_0(\vartheta, \varphi, t)$, when averaged, has a tensor form relating it to the direction of the unit-normal vector $\boldsymbol{n}$ in the following approximate (lowest order) form:

$$\overline{r_0(\vartheta, \varphi, t)} = d_{ij} n_i n_j. \tag{13}$$

The tensor $\boldsymbol{d}$ is the elliptical structure tensor, and the average distance between the particles depends on the direction. The transverse isotropy expected in the present case would impose on $\boldsymbol{d}$ the form:

$$\boldsymbol{d} \Rightarrow \begin{pmatrix} d_{11} & 0 & 0 \\ 0 & d_r & 0 \\ 0 & 0 & d_r \end{pmatrix}, \tag{14}$$

with two coefficients d_{11} and d_r. The fluctuations in $r_0(\vartheta, \varphi, t)$ in both direction and time are denoted by $d^*(t)$, that is $r_0(\vartheta, \varphi, t) = d_{ij} n_i n_j + d^*(t)$. The fluctuations in the distance are also the fluctuations in h, and Eq. 11 therefore becomes

$$\boldsymbol{\sigma}_{ij} = \frac{1}{V_1} \left[\int_{\substack{\text{unit} \\ \text{sphere}}} d\Omega p(\Omega) d_{kl} n_k n_l n_i n_j \frac{\partial V}{\partial h}\bigg|_{\bar{h}} + \frac{1}{2} \int_{\substack{\text{unit} \\ \text{sphere}}} d\Omega p(\Omega) n_i n_j \frac{\partial^2 V}{\partial h^2}\bigg|_{\bar{h}} \overline{(d^*)^2} \right]. \tag{15}$$

This may be further evaluated if any knowledge about $p(\Omega)$ is available.

Case 2: $\kappa^2\overline{(h-\bar{h})^2} \approx 1$. In this case, no series expansion in the potential is possible as this would not lead to a convergent result. Evaluation of Eq. 9 must therefore be carried out directly. This requires knowledge of the pair distribution. The regime is similar to the one that applies to fluids. There is obviously some connection between the functional form of the potential and the structure that materializes in a given flow situation. The problem is discussed in the literature, both for noninteracting particles (Batchelor, 1977) and for interacting particles (Hess, 1980). The Smoluchowski equation is developed in these references for the appropriate flow situation (Rice and Gray, 1965). Cole (1967) lists various approaches to the rate equation that controls the pair distribution function. These equations represent a balance between the chaotic influences that follow from random, isotropic temperature effects and average flow patterns that have an ordering tendency. The former phenomena tend toward isotropic structures, while the latter tend to align the structure with the particle flow-rate tensor. It is uncertain whether this approach is entirely valid for the present experimental setup, as the flow type contains a large component of the phase-velocity difference that is highly directional and thus undermines the concept of isotropic disorder. A new approach to the problem of ascertaining the character of the structure of the directional interparticle distance distribution was presented by Koenders (1995) using continuum mechanics and requiring that the intensity of the fluctuation field neither increase nor decay exponentially in space and time. This approach can only contribute to information on the average structure of the interparticle distance. The preceding are background considerations when the form of the continuum stress is estimated.

The stress is evaluated as in Case 1. The summation sign in Eq. 10 is replaced by an integral, but now no average distance can be employed, thus complicating the form of the distribution function, which is now not just direction dependent but also contains information on the interparticle distance h:

$$\sigma_{ij} = \frac{1}{V_1}\int dh \int_{\substack{\text{unit}\\ \text{sphere}}} d\Omega p(h,\Omega)\frac{\partial V}{\partial h}(2a+h)n_i n_j, \quad (16)$$

where $p(h, \Omega)dhd\Omega$ is the number of particles between surface distances h and $h+dh$ as well as solid angles Ω and $\Omega + d\Omega$ in the vicinity of a representative particle. For the dilute mixtures envisaged here—$0.01 < \phi < 0.1$—the average distance between particle centers in an isotropic packing is roughly $a\phi^{-1/2}$, which makes the spacing between particle surfaces similar to that of the particle diameter.

The pair potential itself has the asymptotic form $V_0 e^{-\kappa(r-2a)}$ when κa is small (that is, < 5), and $-V_0 \ln(1-e^{-\kappa(r-2a)})$ when κa is large (> 10), where V_0 is given in the physical chemistry literature on double-layer interaction as approximately $2\pi\epsilon a\psi_0^2$, where $\epsilon = \epsilon_0\epsilon_r$ is the dielectric permittivity, and ψ_0 is the surface potential (see, for example, Hunter, 1987). Reasonable estimates for these variables are known. Values for κ are given in the same sources.

The evaluation of the integrals in Eq. 16 depends on the form of $p(h, \Omega)$. It has already been argued that the microstructure may be strongly anisotropic and therefore, given the form of the interactive potential, the outcome is dominated by a small number (N_i) of strong interactions in the x-direction. For these interactions the magnitude of the force is approximately κV_0, and h is negligible; the ratio of $(2a+h)/V_1$ is about $a\sqrt{\phi}/V_p$ in magnitude. Thus, for small values of κa, σ_{xx} takes the form:

$$\sigma_{xx} = \frac{-\kappa a}{V_p} N_i V_0 \phi^{1/2} \qquad (\kappa a \text{ small}). \quad (17)$$

Using $\phi V_1 = V_p$, and assuming that N_i is a weak function of the solidosity, the "diffusion parameter" is estimated as

$$\frac{1}{\phi}\frac{\partial \sigma_{xx}}{\partial \phi} \approx \frac{-\kappa a N_i V_0}{2\phi^{3/2} V_p}. \quad (18)$$

An estimate of the variation of h with ϕ is needed for the thin double layer, but as yet no appropriate theory has been developed to produce one. A theory to estimate N_i is also required, and work on modifying existing theories mentioned earlier is in progress.

Case 3: $\kappa^2\overline{(h-\bar{h})^2} \gg 1$. This case describes the situation where, compared to the average interparticle distance, the ζ-potential does not have a noticeable range. The particles behave more or less like the molecules of a gas of hard spheres. The important parameter is now the granular temperature, a measure for the energy of the fluctuations. These fluctuations, when averaged over a time scale that is short in comparison to the overall changes in the medium, span many particle diameters and are thus defined by the fluctuations that reign throughout the medium. The quadratic average gives a constant value. The quadratic displacement in Brownian motion is proportional to the temperature, defined as the quadratic measure of the particles' velocity fluctuations, sometimes called the granular temperature. (It should be noted that the physical origin of the fluctuations need not be Brownian.) Field equations for the granular temperature in a viscous medium are available (McTigue and Jenkins, 1992; Nott and Brady, 1994) and the nonlocal character of the fluctuations is recognized. The kinetic theory developed for dry granular media is a natural vehicle (Bagnold, 1954; Jenkins and Savage, 1983; Gidaspow, 1994). The addition of a viscous medium was made recently (McTigue and Jenkins, 1992; Nott and Brady, 1994). Solutions of the temperature-field differential equations are available for dense media in a state of shear with smooth boundaries. For the present experimental system, the septum–particle–fluid system creates a continually changing distribution of fluid and particle velocity direction and magnitude over the filter cross section, particularly during the initial stages of deposition when pores in the septum are being closed off to fluid in a more or less random way and thereby frequently causing fluid streamlines to deviate. The distance between the pores, the particle size, and the pore sizes are all roughly of the same order. The dominating kinematic feature will be the changes in particle velocities near the septum, and the granular temperature near the

septum is thus reasonably assumed to be proportional to the quadratic velocity difference between particles and fluid. The net force on a particle takes the form:

$$F_i = -\frac{m\nu^2}{\phi}(U-v)^2\frac{\partial\phi}{\partial x_i}, \tag{19}$$

where m is the average mass of the particles and ν gives the factor by which the average phase-velocity difference is amplified to yield a measure for the magnitude of the fluctuations in the fluid velocity. A first-order estimate of ν is the ratio of the cross-sectional area of the cylinder in which the experiment is carried out to the total area of the pores in the septum.

The constitutive behavior of the fluid in the suspension is discussed in Koenders and Williams (1992) for isotropic geometries. The fluid pressure p and the phase velocities are related as follows:

$$-\frac{\partial p}{\partial x} + A(U-v) = 0. \tag{20}$$

The Darcy coefficient A is connected to β by

$$A = -\phi\beta. \tag{21}$$

Higher order terms similar to the one in Eq. 4 can be introduced (Koenders and Williams, 1992), but they have no noticeable effect on the end result of the analysis.

Filtrate Flow Rate Calculation

The aim of the analysis is to calculate the filtrate flow rate, and to gain detailed knowledge of the effects of fundamental variables that characterize the suspension, such as the zeta potential, as well as of the operating parameters of a filter, such as the applied pressure. We do this by solving the equations of continuity, Eqs. 1 and 2, together with a force balance for the particles. The force balance is obtained by equating the drag force, Eq. 4, to an appropriate form of the interparticle repulsion force. The appropriate form is determined by the nature of the interaction: in the case of soft-sphere interactions, this requires the use of Eqs. 9 and 18, and for hard-sphere interactions, Eq. 19. The methods used to solve the resulting equations are given in the Appendix. For the initial stages of filtration ($t \to 0$), and assuming that the solidosity is small, the expression for the flow rate is found to be

$$q(t) = \frac{p}{R(t)} = \frac{p}{R(0)\left(1+\dfrac{\delta R}{R(0)}\right)} = \frac{p}{R(0)}\left[1 - \frac{\delta R}{\delta\phi}\bigg|_{\phi=\phi_0}\frac{2}{R(0)V_T^{n/2-1}}\sqrt{\frac{\beta\phi_0 t}{J_n\pi}}\right]. \tag{22}$$

The piston velocity, V_T, is approximated as $-(p/R(0)A_0)$ to give for the measurable cumulative volume of filtrate Vol(t) produced in the early stages of filtration:

$$\mathrm{Vol}(t) = \frac{p}{R(0)}t - \frac{4}{3}\frac{p}{R(0)^2}\left(\frac{p}{R(0)A_0}\right)^{1-n/2}\sqrt{\frac{\beta\phi_0}{\pi J_n}}\,t^{3/2}\frac{\delta R}{\delta\phi}\bigg|_{\phi=\phi_0}. \tag{23}$$

The two cases of interest are $n = 0$ (soft-sphere interactions) and $n = 2$ (hard-sphere interactions). Writing

$$\mathrm{Vol}(t) = \bar{x}t + \bar{y}t^{3/2} \tag{24}$$

gives

$$\bar{x} = \frac{p}{R(0)} \quad \text{and} \quad \bar{y} = -\frac{4}{3}\frac{p^2}{A_0R(0)^3}\sqrt{\frac{\beta\phi_0}{\pi J_0}}\frac{\delta R}{\delta\phi}\bigg|_{\phi=\phi_0} \quad (n=0) \tag{25}$$

$$\bar{x} = \frac{p}{R(0)} \quad \text{and} \quad \bar{y} = -\frac{4}{3}\frac{p}{R(0)^2}\sqrt{\frac{\beta\phi_0}{\pi J_2}}\frac{\delta R}{\delta\phi}\bigg|_{\phi=\phi_0} \quad (n=2). \tag{26}$$

Thus, the behavior for the two cases is quite different. These equations can be verified by creating experimental conditions that correspond to cases 2 and 3. This is mainly achieved by varying the ζ-potential.

Experiments

Suspensions were prepared for the filtration experiments using anatase (supplied by Tioxide PLC) suspended in double distilled water. Particles were washed initially by dispersing them in water and shaking the mixture using a flask shaker until the liquid conductivity reached a constant value. The particles were allowed to settle, and excess liquid was decanted off. This washing and decanting process was repeated several times until the solution conductivity was the same from one decant to the next. The solids volume fraction was then adjusted to that required for the experiment, and the pH altered by the addition of HCl or NaOH, as appropriate.

The size distribution of the particles was measured using a Malvern Mastersizer, and their zeta potentials determined using a Malvern Zetasizer. The isoelectric point of the particles occurred close to pH 3.4, suggesting that the anatase was in a coated form. The particle-size distribution had a mean surface-volume equivalent diameter of 0.5 μm and a size range from 0.1 to about 5 μm, indicating that the particles were probably not fully dispersed by the mixing techniques used. Nonetheless, the same technique was used from one experiment to the next, and the same reproducible size distribution was obtained prior to pH adjustment of the suspension.

The filtration tests were carried out in a piston press which comprised an upright, polished stainless-steel cylinder mounted on a circular base. The cylinder had an internal bore of 43 mm and a height of 193 mm (107 mm in some experiments). The base contained a 43-mm diameter recess into which a loosely fitting stainless-steel sinter disc was inserted; this disc supported a porous nylon membrane (0.1 μm Pall

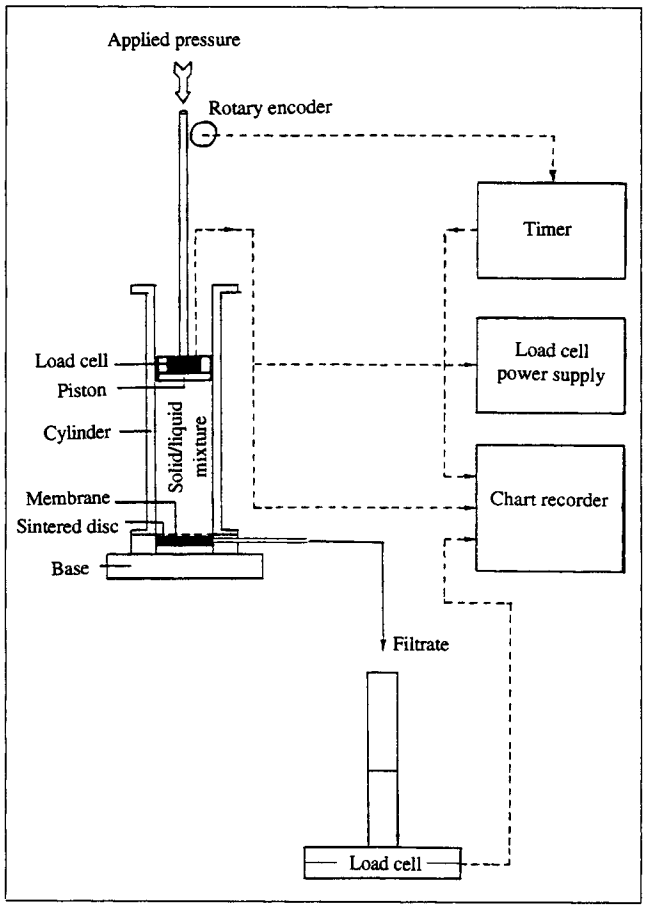

Figure 2. Experimental apparatus.

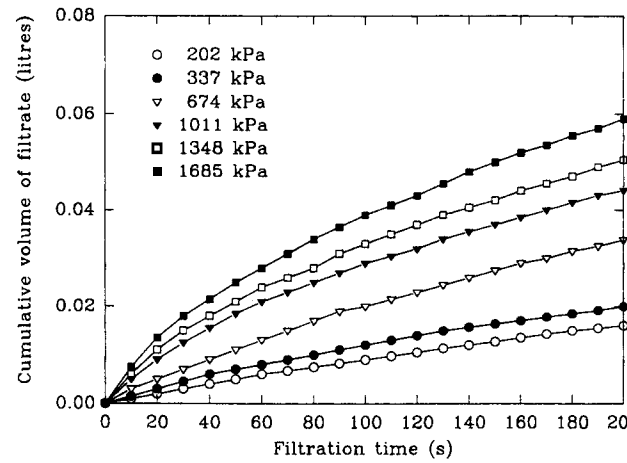

Figure 3. Cumulative volume of filtrate as a function of the filtration time at various piston pressures.

Posidyne) onto which a cake was deposited. At the start of an experiment the cylinder was filled completely with suspension, the piston brought into contact with the suspension surface, and then the load was applied to the piston (and maintained constant) using a controlled pneumatic cylinder fed from a compressor. The mass of liquid draining through the membrane was recorded using a load cell connected to a data acquisition system. The applied pressure was monitored via a load cell mounted in the piston head. The overall arrangement of the apparatus is shown in Figure 2.

A typical set of experimental data, plotted as the volume of filtrate collected as a function of the filtration time, is shown in Figure 3 for a range of applied pressures. In order to examine cases 2 and 3 (case 1, where the particles are initially more or less at rest in a dense packing, is a special case that rarely occurs in applied filtration problems and was not considered from the experimental viewpoint), discussed in the theoretical investigation, an appropriate range of variables was chosen. The variables selected for study were the initial volume fraction of solids in the suspension (ϕ), the pressure applied at the suspension surface (p), and the zeta potential of the particles in suspension (ζ).

Evaluation of experiments

The data are fitted to volume–time curves of the form $\mathrm{Vol}(t) = \bar{x}t + \bar{y}t^{3/2}$. For the theoretical analysis to be valid, the increase in the solidosity must be small. The parameters $\bar{x}$ and $\bar{y}$ are determined by means of a least-squares routine from the initial stages of each experiment. The details of the routine are described by Topping (1972), who also calculated an error measure for the values of $\bar{x}$ and $\bar{y}$ based on the statistical distribution of the data points around the curve. Another error measure can be obtained by comparing various lengths of the time record. In both cases, the errors in $\bar{x}$ are mostly small and not always shown in the graphs of the results. The errors in $\bar{y}$ are experiment dependent and given on the graphs of the results; generally speaking they are larger, ranging from some 10% to an order of magnitude.

The experiments are classified on the basis of the expected value of the parameter $\kappa^2\overline{(h-\bar{h})^2}$. The value of κ is estimated from the measured electrical properties of the particles and the ionic composition of the fluid, and an estimate of the value of $\bar{h}$ is calculated from the average interparticle distance. The value of $\bar{h}$ is roughly $a\phi^{-1/2} - 2a$ for a monodisperse distribution of sizes and low values of the solidosity. For a heterodisperse size distribution the radius of the average particle by number $\langle a \rangle$ is used; for the experiments considered here it is found that $\langle a \rangle \approx 0.1$ μm. The condition $\kappa^2\overline{(h-\bar{h})^2} = O(1)$ is satisfied in the range of solid volume fractions $0.02 < \phi < 0.1$, and κ^{-1} is on the order of 50 nm. In this range the pressure dependence of $\bar{y}$ is quadratic (see Eq. 25).

For the experiments that satisfy $\kappa^2\overline{(h-\bar{h})^2} \gg 1$, the pressure dependence of $\bar{y}$ is expected to be linear (Eq. 26), and the solidosity dependence of J_2 will then be approximately proportional to ϕ^{-1} (Eq. A3). This regime can be found either for low values of the solidosity or for large κ or for small values of the ζ-potential. The latter two factors are mostly satisfied simultaneously.

Finally the case $\kappa^2\overline{(h-\bar{h})^2} \ll 1$ will be of interest, which is only found for solidosities in the range $\phi > 0.1$, and the analysis set out in the Appendix is thus not valid. This case has a number of quite unique peculiarities, and therefore the measurements that apply to it are left to a later report.

The following parameter ranges are considered below, with experimental data appropriate to each set of conditions:

• I. The case of $\kappa^2\overline{(h-\bar{h})^2} = O(1)$ for various values of ϕ at constant pressure.

• II. The case of $\kappa^2\overline{(h-\bar{h})^2} = O(1)$ at $\phi = 0.01$ for a range of pressures.

• III. The case of $\kappa^2\overline{(h-\bar{h})^2} \gg 1$ for a range of pressures at $\phi = 0.01$ at constant pressure.

• IV. The case of $\kappa^2\overline{(h-\bar{h})^2} \gg 1$ for various values of ϕ at a constant pressure.

To study the experiments with a view of deriving numerical estimates of the diffusion parameter in various circumstances it is necessary to have an idea of the behavior of $\bar{x}$. The accumulation of particles on the septum causes clogging, and as a result the septum permeability is reduced. The magnitude of this effect is directly expressed in $\bar{x}$. In Figure 4 the value of $\bar{x}$ is plotted as a function of the solidosity at $p = 337$ kPa and $\zeta = -44$ mV. A functional relationship will be required later on, but it is seen that no simple power law fits the whole range of solidosities. It is also noted that a distinct turnover in behavior occurs at $\phi \approx 10^{-3}$.

I. The values for $\bar{x}$ in the range $0.01 < \phi < 0.1$ are plotted (Figure 4) and fitted to the expression:

$$\ln\left(\frac{\bar{x}^2}{2}\right) = -1.14\ln^2(\phi) - 9.73\ln(\phi) - 52.5. \qquad (27)$$

The value of J_0 follows from Eq. 25, $n = 0$:

$$J_0 = \left(\frac{\delta(\bar{x}^2/2)}{\delta\phi}\right)^2 \frac{16\beta\phi_0}{9\pi A_0^2 \bar{y}^2}. \qquad (28)$$

The main sources of error in the experimental determination of J_0 are the errors in $\bar{x}$ and $\bar{y}$. These have a large impact on Eq. 28 because of the high exponential order in which these variables occur. Generally speaking the order of the error $\bar{x}$ and $\bar{y}$ is some 30%, and therefore only an order of magnitude for J_0 can be achieved. Although the model predictions as obtained from the theoretical investigation are equally rough, some comparison can be made. Three theoretical estimates for J_0 are derived, the first from Eq. 18; the second from Eq. 15 in isotropic packing at $h \approx a\phi^{-1/2} - 2a$, which yields the result

$$J_0 = \frac{N_i V_0 \kappa a\left(a\kappa + \sqrt{\phi}\right)e^{-a\kappa(\sqrt{\phi}-2)}}{2V_p\phi^2}; \qquad (29)$$

and the third is an upper bound, evaluating the force contribution in Eq. 29 in $h = 0$:

$$J_0 = \frac{N_i V_0 \kappa a\left(a\kappa + \sqrt{\phi}\right)}{2V_p\phi^2}. \qquad (30)$$

The potential front factor is calculated from $V_0 = 2\pi\epsilon_0\epsilon_r a\psi_0^2$, with a value of $\epsilon_r = 80$ and the surface potential $|\psi_0| = 40$ mV. N_i is chosen equal to 6.

The three estimates are shown in Figure 5 for two values of $b = \kappa\langle a\rangle$. It is observed that the estimate obtained from case 1 is only relevant for high values of the solidosity. Experimental values are also obtained. There are three experiments that qualify: $\phi = 0.01$; $\phi = 0.025$; and $\phi = 0.1$. For the analysis β must be given (Eq. 28), and this quantity depends strongly on the choice of $\langle a\rangle$ and is furthermore influenced by the anisotropy of the packing (the estimates discussed in the theoretical investigation only pertain to isotropic microstructure, but anisotropy may have a substantial impact). Thus an upper bound for J_0 on the order of 10^7 $Nm^{-1}s^{-1}$ is found, more or less independent of the solidosity. A lower bound may be as much as a factor of 20 smaller.

The comparison between theory and experiment permits a rough estimate of b: $b = 1$–10, a value that corresponds to a double layer thickness of $\kappa^{-1} \approx 10$–100 nm. This value is in the order of magnitude that is expected: 50 nm $< \kappa^{-1} <$ 500 nm. However, various elements of the theory are deficient: granular temperature effects have been neglected; the pair potential is approximate (some 40% error may be expected, Hunter, 1987); and for the lower solidosity, $\phi = 0.01$, the theory is also not entirely valid because the condition $\kappa^2\overline{(h-\bar{h})^2} = O(1)$ is not completely satisfied.

II. This case is used to prove the assumption that the clogged septum permeability depends only on the solidosity. $\bar{x}$ is plotted as a function of the applied pressure for $\zeta = -44$ mV (Figure 6). A regression analysis on the data shows that $\bar{x} \propto p^{1.01}$, so that it may be concluded that the resistance is constant with respect to the flow velocity and only depends on the solidosity near the septum.

A quadratic dependence of $\bar{y}$ on the piston pressure p is expected (Eq. 25). The relevant data (for $\zeta = -44$ mV) are plotted in Figure 7. The agreement with the theory is not perfect; the regression line follows the curve $\bar{y} \propto p^{1.7}$, but no perfect agreement is expected because for $\phi = 0.01$ neither a random temperature model nor a fixed interparticle distance model is genuinely valid.

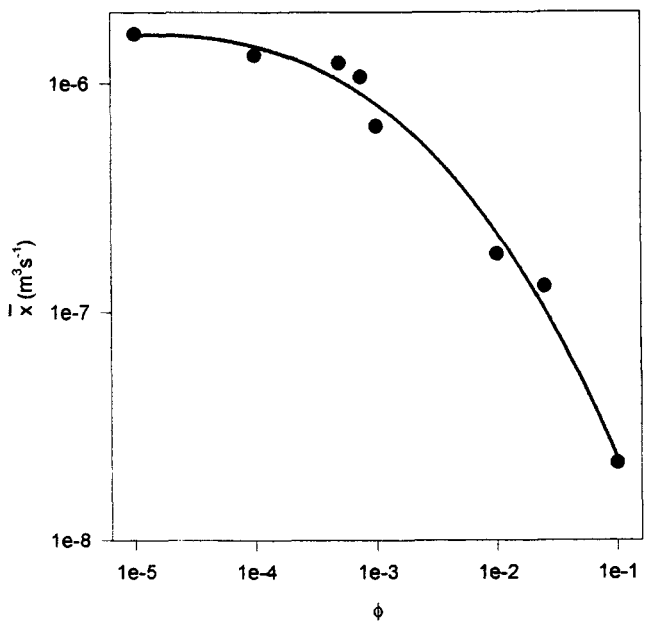

Figure 4. Value of $\bar{x}$ as a function of the solidosity at $\zeta = -44$ mV and piston pressure of 337 kPa.

The experiments in the range $0.01 < \phi < 0.1$ are fitted to $\ln(\bar{x}^2/2) \approx -1.14\ln^2(\phi) - 9.73\ln(\phi) - 52.5$.

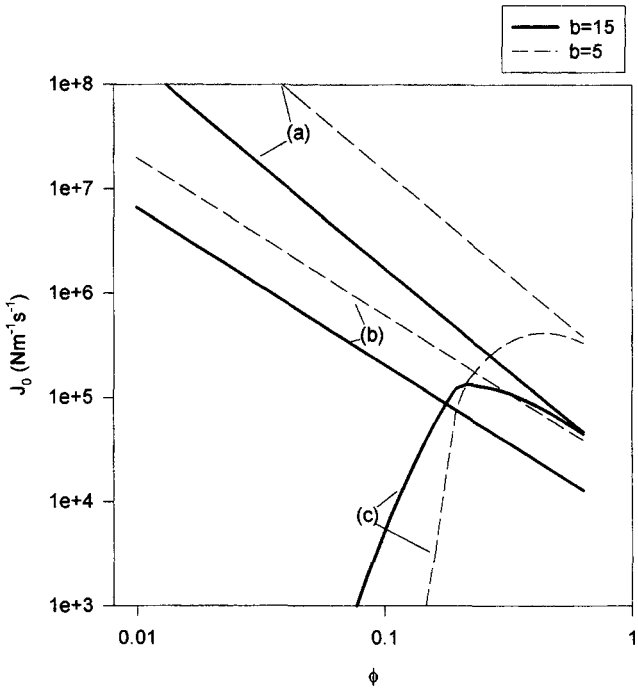

Figure 5. Theoretical estimates of the parameter J_0.

(a) According to the upper limit of Case 1

$$J_0 = \frac{N_i V_0 \kappa a(a\kappa + \sqrt{\phi})}{2V_p \phi^2},$$

(b) According to Case 2

$$J_0 = \frac{a\kappa N_i V_0}{2\phi^{3/2} V_p},$$

(c) According to Case 1 in isotropic packing

$$J_0 = \frac{N_i V_0 \kappa a(a\kappa + \sqrt{\phi}) e^{-a\kappa(\sqrt{\phi}-2)}}{2V_p \phi^2}.$$

The surface distance between particles is given by $h \approx a\phi^{-1/2} - 2a$, $N_i = 6$, the potential front factor $V_0 = 2\pi\epsilon_0\epsilon_r a\psi_0^2$, with $\epsilon_r = 80$ and $|\psi_0| = 44$ mV, $\langle a \rangle = 1.1 \times 10^{-7}$ m, and $b = \kappa\langle a \rangle$.

III. This case is achieved by making the ζ-potential low. A linear pressure dependence of $\bar{y}$ is expected. The data for $\zeta = 0$ mV are plotted in Figures 6 and 7. A regression analysis yields $\bar{y} \propto p^{1.07}$. The data for $\bar{x}$ are also fitted; the exponent for the pressure depended a great deal on the location of the value for $p = 0.3$ MPa and this data point is very noisy. In general there are quite wide fluctuations in the time–volume plots for the data used in this case. Although the lack of an interactive potential apparently makes the process much more unstable, the general trend is clear and it follows the theoretical principles outlined in this article.

IV. Two sets of data are available for this case; the first has high ζ-potential, but very low ϕ (on the order of 10^{-3}–10^{-5}); the second has negligible ζ-potential and $10^{-3} < \phi < 2.5 \times 10^{-2}$. Both sets of data satisfy $\kappa^2(h - \bar{h})^2 \gg 1$. In

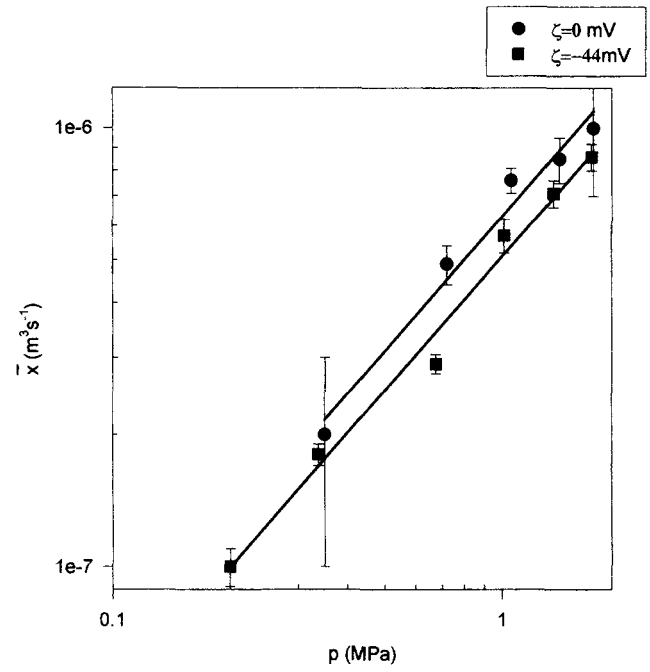

Figure 6. Value of $\bar{x}$ as a function of the filtration pressure at $\zeta = 0$ and –44 mV at $\phi = 0.01$.

order to derive features of J_2, the derivative of $\bar{x}$ with respect to ϕ is needed. $\bar{x}$ is plotted for the two sets of data in Figures 4 and 8; $\bar{x}$ is approximated as

$$\bar{x} = a_x \phi^{b_x}. \tag{31}$$

Similarly $\bar{y}$ is approximated as

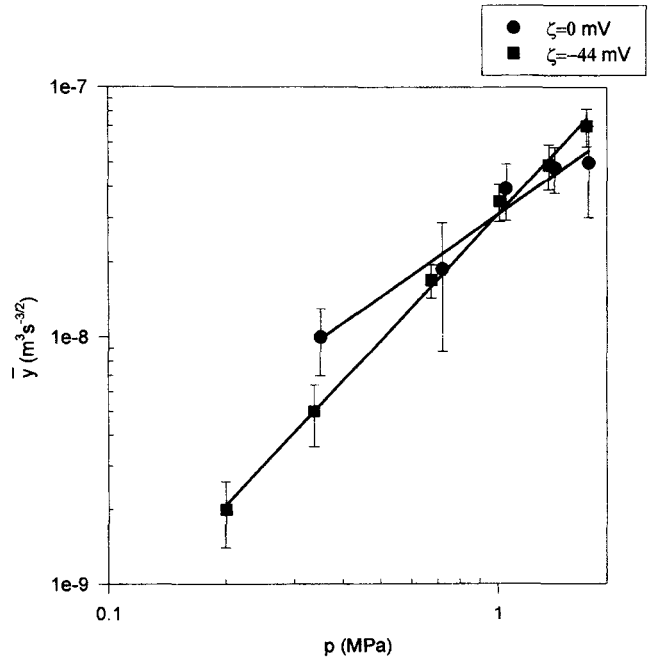

Figure 7. Value of $\bar{y}$ as a function of the piston pressure at $\zeta = 0$ and –44 mV at $\phi = 0.01$.

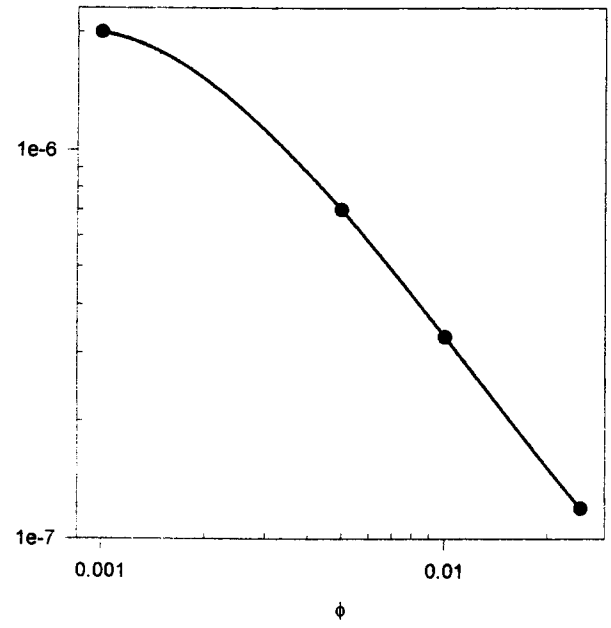

Figure 8. Value of $\bar{x}$ as a function of the solidosity at $\zeta \approx 0$ mV and piston pressure of 337 kPa.

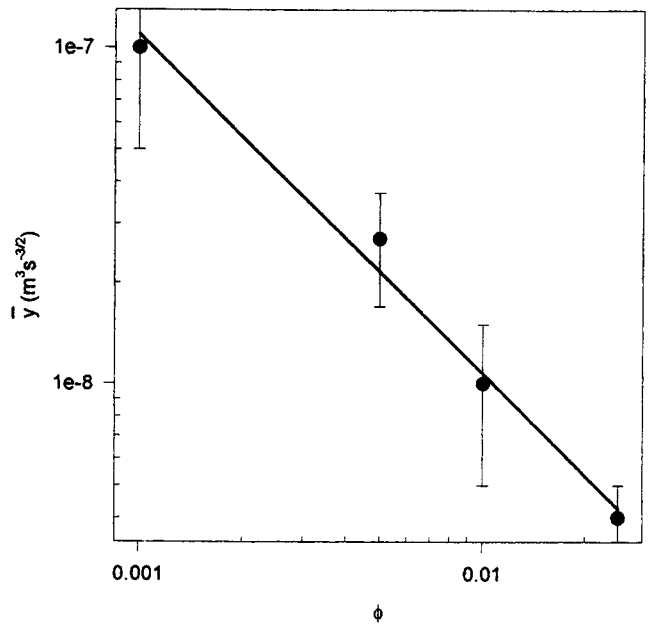

Figure 10. Value of $\bar{y}$ as a function of the solidosity at $\zeta \approx 0$ mV and piston pressure of 337 kPa.

$$\bar{y} = a_y \phi^{b_y}. \tag{32}$$

From Eq. 26, $n = 2$, it follows that

$$J_2 = \frac{16\beta}{9\pi} \frac{a_x^2 b_x^2}{a_y^2} \phi_0^{-2b_y + 2b_x - 1}. \tag{33}$$

The two sets of data for $\bar{y}$ are plotted in Figures 9 and 10; a regression analysis is carried out to obtain the estimates for a_y and b_y. In the same way, a_x and b_x are found. There are obviously quite substantial error margins, but the whole range of tests gives a good indication of the trend in the data. For the set with $\zeta = -44$ mV and $10^{-5} < \phi < 10^{-3}$, it is found that $\bar{x} = 10^{-6.5}\phi^{-0.15}$ and $\bar{y} = 10^{-8.4}\phi^{-0.23}$. For the measurement set with $\zeta = 0$ mV and $10^{-3} < \phi < 2.5 \times 10^{-2}$, the corresponding result is $\bar{x} = 10^{-8.7}\phi^{-1.1}$ and $\bar{y} = 10^{-10.0}\phi^{-1.0}$. The associated solidosity dependence for the coefficient J_2 is $J_2 = 140(16\beta/9\pi)\phi^{-0.85}$ for the former series and $J_2 = 480(16\beta/9\pi)\phi^{-1.2}$ for the latter. These results are similar in the range of ϕ considered here. Also in both cases, the exponent of ϕ is close to -1, which is what the theory suggested. So even while the experimental error is quite large, very reasonable results are obtained, as expected for very low solids concentrations.

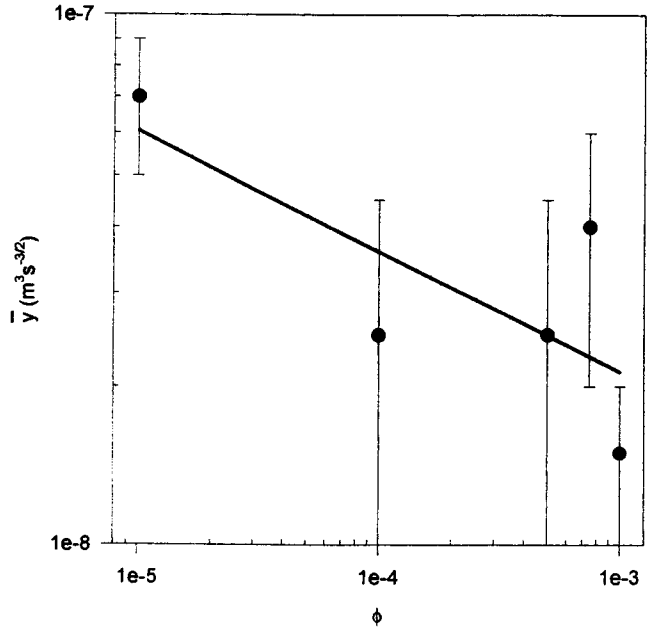

Figure 9. Value of $\bar{y}$ as a function of the solidosity at $\zeta = -44$ mV and piston pressure of 337 kPa.

The experimental value for J_2 permits the estimate of the factor ν in Eq. A3. The average particle mass is of the order of 5×10^{-18} kg, resulting in a value for $\nu \approx 1.0 \times 10^5$ (using the viscosity of the water at room temperature and a particle radius on the order of 10^{-7} m). The pore radius of the septum is measured to be on the order of 10^{-7} m. Now if ν is approximated as the ratio of the cylinder cross section to the total pore surface available to flow, the number of pores per mm^2 is estimated as in the order of 5×10^2, and the clean water value for the septum is of the order of $10^{7.5}$. If the effective pore size is assumed to be slightly smaller, 10^{-8} m, then the number of pores per mm^2 is 4×10^4, which is a very reasonable value. The factor ν of course contains more than just the pore area to cylinder cross-sectional ratio; it also says something about the efficiency with which velocity fluctuations are transmitted to the particles.

Conclusions

Filtration models have generally failed to recognize the role of interparticle forces during cake formation and consolida-

tion, although experimental evidence pointing to its importance has been recognized. The simplest theories for constant-pressure filtration of noninteracting particles arrive at the conclusion that the filtrate volume produced is proportional to $p^{0.5}$, and that any particle–particle interaction effect has been accounted for empirically. This work has shown that the relationship of filtrate volume produced during the initial stages of cake formation by pressure is dependent on the range of the zeta potential; analytical solutions are presented for soft-sphere and hard-sphere interactions. The modeling approach is based on established theories for suspension flow, and it shows the differences in the physical character between dilute suspensions of strongly interacting particles and dilute systems of relatively free particles. While the behavior of the latter is dominated by fluctuations of particle velocities near the septum, in the former type of suspension the particle behavior is localized. Unlike previous developments, the present work gives a fundamental understanding and insight into the role of interactions in filtration.

Previous work has not separated out and studied the initial stages separately from the cake formation (i.e., after the septum effects have diminished) and consolidation stages, in spite of apparently inexplicable filtration data relating to the early stage of filtration that exist in the literature relating to fine-particle systems. A complete analysis of the cake formation process can now be developed to account for both the initial and subsequent stages.

Acknowledgments

The authors thank the Engineering and Physical Sciences Research Council and the International Fine Particle Research Institute for research grants in support of this work.

Notation

$A(s)$ = Laplace amplitude of the solidosity
a_x, a_y = curve-fit parameters in Eqs. 31 and 32
$b = b = \kappa\langle a\rangle$
b_x, b_y = curve-fit parameters in Eqs. 31 and 32
$d^*(t)$ = fluctuations in the distance between particles
$D(t)$ = superficial velocity at the septum
J_0 = proportionality constant of the diffusion coefficient for systems where the direct interaction between the particles is dominant
J_2 = proportionality constant of the diffusion coefficient for systems where the fluctuations in particle motion is dominant
k_1, k_2 = front factors in the power laws to describe Buscall and White's (1987) compressive yield stress
n = power coefficient introduced in Eq. A1 to distinguish between the cases of hard- and soft-sphere interaction
n_1, n_2 = power-law coefficients to describe Buscall and White's (1987) compressive yield stress
N = suspension compressibility coefficient
$q(t)$ = time-dependent fluid flow rate
s = Laplace frequency
x = spatial coordinate, beginning at the septum surface
$\bar{x}$ = initial linear flow rate (see Eq. 24)
$\bar{y}$ = coefficient denoting the lowest order change in the initial linear flow rate (see Eq. 24)
ϕ_0 = solidosity of the feed suspension
ϕ^+ = variation in the solidosity at the initial stage
$\lambda_{1,2}$ = solutions of the secular equation (Eq. A16)
τ = time
ϑ, φ = spherical angular coordinates
Ω = solid angle

Literature Cited

Abramowitz, M., and I. A. Stegun, *Handbook of Mathematical Functions*, 9th ed., Dover, New York (1972).
Auzerais, F. M., R. Jackson, and W. B. Russel, "The Resolution of Shocks and the Effects of Compressible Sediments in Transient Settling," *J. Fluid Mech.*, **195**, 437 (1988).
Bagnold, R. A., "Experiments on a Gravity-free Dispersion of Large Solid Spheres in a Newtonian Fluid Under Shear," *Proc. R. Soc. Lond.*, **A225**, 49 (1954).
Batchelor, G. K., "The Effect of Brownian Motion on the Bulk Stress in a Suspension of Spherical Particles," *J. Fluid Mech.*, **83**(1), 97 (1977).
Buscall, R., and L. R. White, "The Consolidation of Concentrated Suspensions—The Theory of Sedimentation," *J. Chem. Soc. Faraday Trans. 1*, **83**, 873 (1987).
Cole, G. H. A., *An Introduction to the Statistical Mechanics of Simple Dense Fluids*, Pergamon, Oxford (1967).
Gidaspow, D., *Multiphase Flow and Fluidization*, Academic Press, San Diego (1994).
Happel, J., and H. Brenner, *Low Reynolds Number Hydrodynamics*, Kluwer, Dordrecht, The Netherlands (1973).
Hess, S., "Shear-Flow Induced Distortion of the Pair-Correlation Function," *Phys. Rev. A*, **22**(6), 2844 (1980).
Howells, I., K. A. Landman, A. Panjkov, C. Sirakoff, and L. R. White, "Time-Dependent Batch Settling of Flocculated Suspensions," *Appl. Math. Model.*, **14**, 77 (1990).
Hunter, R. J., *Foundation of Colloid Science*, Vol. I, Clarendon, Oxford (1987).
Jenkins, J. T., and S. B. Savage, "A Theory for Rapid Flow of Identical, Smooth, Nearly Elastic Spherical Particles," *J. Fluid Mech.*, **130**, 187 (1983).
Koenders, M. A., "Techniques for Ultra-Heterogeneous Materials," *Proc. Joint Applied Mechanics and Materials Summer Conf.*, ASME, New York, p. 14 (1995).
Koenders, M. A., and R. J. Wakeman, "The Initial Stages of Compact Formation from Suspensions by Filtration," *Chem. Eng. Sci.*, **51**, 3897 (1996).
Koenders, M. A., and A. F. Williams, "Flow Equations for Particle Fluid Mixtures," *Acta Mech.*, **92**, 91 (1992).
Landman, K. A., and W. B. Russel, "Filtration at Large Pressures for Strongly Flocculated Suspensions," *Phys. Fluids A*, **5**, 550 (1993).
Landman, K. A., C. Sirakoff, and L. R. White, "Dewatering of Flocculated Suspensions by Pressure Filtration," *Phys. Fluids A*, **3**, 1495 (1991).
Landman, K. A., L. R. White, and R. Buscall, "The Continuous-Flow Gravity Thickener: Steady State Behavior," *AIChE J.*, **34**, 239 (1988).
Landman, K. A., L. R. White, and M. Eberl, "Pressure Filtration of Flocculated Suspensions," *AIChE J.*, **41**, 1687 (1995).
Landman, K. A., and L. R. White, "Determination of the Hindered Settling Factor for Flocculated Suspensions," *AIChE J.*, **38**, 184 (1992).
Leu, W., "Principles of Compressible Cake Filtration," *Encyclopedia of Fluid Mechanics*, Vol. 5, N. P. Cheremisinoff, ed., Gulf Pub., Houston (1986).
McTigue, D. F., and J. T. Jenkins, "Channel Flow of a Concentrated Suspension," *Advances in Micromechanics of Granulet Materials*, H. H. Shen et al., eds., Elsevier, Amsterdam (1992).
Murdoch, A. I., "The Motivation of Continuum Concepts and Relations from Discrete Considerations," *Q. J. Mech. Appl. Math.*, **36**, 2. 163 (1983).
Nott, P. R., and J. F. Brady, "Pressure Driven Flow of Suspensions: Simulation and Theory," *J. Fluid Mech.*, **275**, 157 (1994).
Ottewill, R. H., "Direct Measurements of Particle-Particle Interactions," *Progr. Colloid Polym. Sci.*, **67**, 71 (1980).
Rice, S. A., and P. Gray, *The Statistical Mechanics of Simple Liquids*, Interscience, New York (1965).
Shirato, M., T. Murase, E. Iritani, F. M. Tiller, and A. F. Alciatore, "Filtration in the Chemical Process Industry," *Filtration*, M. J. Matteson and C. Orr, eds., Dekker, New York (1986a).
Shirato, M., T. Murase, M. Iwata, and T. Kurita, "Principles of Expression and Design of Membrane Compression-Type Filter Press Operation," *Encyclopedia of Fluid Mechanics*, Vol. 5, N. P. Cheremisinoff, ed., Gulf Pub., Houston (1986b).

Smiles, D. E., "Principles of Constant Pressure Filtration," *Encyclopedia of Fluid Mechanics*, Vol. 5, N. P. Cheremisinoff, ed., Gulf Pub., Houston (1986).
Tiller, F. M., "Compressible Cake Filtration," *The Scientific Basis of Filtration*, K. J. Ives, ed., Noordhoff, Leyden, The Netherlands (1975).
Topping, J., *Errors of Observation and Their Treatment*, Chapman & Hall, London (1972).
Torquato, S., B. Lu, and J. Rubinstein, "Nearest-Neighbor Distribution Functions in Many-Body Systems," *Phys. Rev. A*, **41**, 2059 (1990).
Wakeman, R. J., "Theoretical Approaches to Thickening and Filtration," *Encyclopedia of Fluid Mechanics*, Vol. 5, N. P. Cheremisinoff, ed., Gulf Pub., Houston (1986).

Appendix: Solution of the Flow Equations

The flow equations are solved below for the initial stage of filtration in a similar way to that applied by Koenders and Wakeman (1996), but the theory is extended to deal with the alternative form of the diffusion coefficient implied in Eq. 19.

The suspension in the filter has a uniform solids volume fraction ϕ_0 at time $t = 0$ when the pressure is first applied. The value of ϕ then changes as a function of time and space to create a gradient at the septum. The initial changes $\phi^+(x,t)$ are small compared to the initial uniform value ϕ_0: $\phi(x,t) = \phi_0 + \phi^+(x,t)$.

The constitutive equation for dilute suspensions is obtained by equating the drag force (Eq. 3) to the appropriate form of the interparticle repulsion force. For the case of soft-sphere interactions this involves Eqs. 9 and 18, and for hard-sphere interactions, Eq. 19. The result can be summarized as follows:

$$\beta(U - v) - J_n(U - v)^n \frac{\partial \phi}{\partial x} = 0, \tag{A1}$$

where $n = 0$ and $n = 2$ apply to the soft-sphere and hard-sphere interactions, respectively. When $n = 0$ holds, the interaction is given by the derivative of the potential (Eq. 18):

$$J_0 = \frac{1}{\phi}\frac{\partial \sigma_{xx}}{\partial \phi} \approx \frac{a\kappa N_i V_0}{2\phi^{3/2} V_p}. \tag{A2}$$

Equation 19 holds for $n = 2$:

$$J_2 = \frac{m\nu^2}{\phi V_p}. \tag{A3}$$

The higher order term given by Eq. 4 is neglected. For the case $n = 0$, the boundary and initial conditions are:

Solidosity at $t = 0$: $\phi(x,0) = \phi_0$ (A4)

Particle velocity at $x = 0$: $v(0,t) = 0$ (A5)

Phase velocity difference at large x: $(U - v)(\infty,t) = 0$ (A6)

Density gradient at large x: $\frac{\partial \phi}{\partial x}(\infty,t) = 0$ (A7)

Velocities at large x: $U(\infty,t) = v(\infty,t) = V_T$, the piston velocity. (A8)

The emphasis is on small initial solidosities ($\phi_0 \sim 0.001$–0.1), and therefore the fluid pressure drop in the suspension is a higher order effect. The permeability is defined by specifying the ratio of the flow rate through the septum to the pressure difference across this device. In the chosen variable set, this is expressed as

$$D(t) = [1 - \phi(0,t)]U(0,t) = -\frac{p}{R(t)A_0}, \tag{A9}$$

where A_0 is the septum area, and $R(t)$ is the resistance of the septum after some particle deposition has taken place. This definition of septum resistance is related to its thickness L, area A_0, and permeability k, and to the fluid viscosity μ through the relationship $R = (\mu L/kA_0)$. This value changes when particles settle onto it; the simplest "law" to describe the evolution of $R(t)$ is to make it dependent on the solidosity at the septum surface $\phi(0,t)$. For the small variations envisaged in the initial stage, the variation in the resistance is evidently

$$\delta R(t) = \left.\frac{\delta R}{\delta \phi}\right|_{\phi_0} \phi^+(0,t). \tag{A10}$$

It is easily verified that in the limit $\phi^+(x,t) \ll \phi_0$; $\phi_0 \ll 1$, the following estimate can be made:

$$(U - v)^2 \frac{\partial \phi}{\partial x} \approx V_T^2 \frac{\partial \phi^+}{\partial x}. \tag{A11}$$

It follows from the equations of continuity and condition A8 that:

$$U - v = \frac{V_T + \frac{1}{\phi}\frac{\partial}{\partial t}\int_0^x \phi^+(x',t)\,dx'}{1 - \phi}. \tag{A12}$$

The constitutive equation A1 takes the following approximated linear form:

$$\beta \frac{\partial \phi^+}{\partial t} + \beta V_T \frac{\partial \phi^+}{\partial x} - J_n V_T^n \phi_0 \frac{\partial^2 \phi^+}{\partial x^2} = 0. \tag{A13}$$

The front factor V_T^n is seen to be independent of the position, and therefore in this approximation it does not matter whether it is a local or nonlocal variable. Equation A13 is Laplace transformed using the initial condition $\phi^+(x,0) = 0$:

$$\beta s\hat{\phi} + \beta V_T \frac{\partial \hat{\phi}}{\partial x} - J_n V_T^n \phi_0 \frac{\partial^2 \hat{\phi}}{\partial x^2} = 0. \tag{A14}$$

Equation A14 is solved for $\hat{\phi}(x,s)$; the solution is

$$\hat{\phi}(x,s) = A(s)e^{\lambda_1 x} + B(s)e^{\lambda_2 x}, \tag{A15}$$

where the values for λ are given by

$$\lambda_{1,2} = \frac{\sqrt{\beta}\left(\pm\sqrt{V_T^2\beta + 4V_T^n J_n \phi_0 s} + V_T\sqrt{\beta}\right)}{2V_T^n \phi_0 J_n}. \quad \text{(A16)}$$

The signs of the constants are $J_n > 0$, $V_T < 0$, and $\beta > 0$. To get finite answers for large x, the implication is that only negative λ represents a physically realistic situation; thus,

$$\hat{\phi}(x,s) = A(s)\exp\left(\frac{-x\sqrt{\beta}\left(\sqrt{V_T^2\beta + 4V_T^n J_n \phi_0 s} + V_T\sqrt{\beta}\right)}{2V_T^n \phi_0 J_n}\right). \quad \text{(A17)}$$

To obtain $A(s)$, Eq. A1 at $x = 0$ is considered. Laplace transforming and substituting condition $v = 0$ (Eq. A5) at $x = 0$, as well as the initial conditions and the approximation that ϕ^+ is small, gives

$$\frac{\beta V_T}{s} - J_n V_T^n \left.\frac{\partial \hat{\phi}}{\partial x}\right|_{x=0} = 0. \quad \text{(A18)}$$

Substitution of the solution (Eq. A16) gives the following form for $A(s)$:

$$A(s) = \frac{2\phi_0 V_T \sqrt{\beta}}{s\left(V_T\sqrt{\beta} - \sqrt{V_T^2\beta + 4V_T^n \phi_0 J_n s}\right)}. \quad \text{(A19)}$$

This is, in fact, the Laplace transform of the accumulation of the solidosity at the septum $\phi^+(0,t)$. The inverse transform is easily obtained (see Abramowitz and Stegun, 1972):

$$\phi^+(0,t) = \sqrt{\frac{\phi_0 \beta}{J_n V_T^{n-2}}} \times \int_0^t d\tau \exp\left(\frac{-\beta\tau}{4\phi_0 J_n V_T^{n-2}}\right) \times \left\{\frac{1}{\sqrt{\pi\tau}} + \sqrt{\frac{\beta}{4\phi_0 J_n V_T^{n-2}}} \exp\left(\frac{\beta\tau}{4\phi_0 J_n V_T^{n-2}}\right) \times \operatorname{erfc}\left(-\sqrt{\frac{\beta\tau}{4\phi_0 J_n V_T^{n-2}}}\right)\right\}. \quad \text{(A20)}$$

For short times, this behaves as:

$$\phi^+(0,t) \approx 2\sqrt{\frac{\phi_0 \beta t}{\pi J_n V_T^{n-2}}}. \quad \text{(A21)}$$

The case $n = 0$ has already been treated by Koenders and Wakeman (1996). For $n = 2$, the hard-sphere case, it is seen that the accumulation at the septum does not depend on the piston velocity, and is therefore independent of the applied pressure.

Calculation of the flow rate is made by assuming that the solidosity is small, and using Eqs. A9, A10, A21:

$$q(t) = \frac{p}{R(t)} = \frac{p}{R(0)\left(1 + \frac{\delta R}{R(0)}\right)} = \frac{p}{R(0)}\left[1 - \left.\frac{\delta R}{\delta \phi}\right|_{\phi=\phi_0} \frac{2}{R(0)V_T^{n/2-1}}\sqrt{\frac{\beta\phi_0 t}{J_n \pi}}\right]. \quad \text{(A22)}$$

Manuscript received Mar. 29, 1996, and revision received Nov. 4, 1996.